THERMAL MODELLING OF PHOTOVOLTAIC MODULES IN OPERATION AND PRODUCTION

Max Mittag, Lennart Vogt, Christoph Herzog, Andrea Pfreundt, Jibran Shahid, Dirk Holger Neuhaus, Harry Wirth
Fraunhofer Institute for Solar Energy Systems ISE, Heidenhofstr. 2, 79110 Freiburg, Germany
max.mittag@ise.fraunhofer.de

ABSTRACT: The temperature of solar cells in photovoltaic modules has a major influence on module power. The module setup, the material structure and the material properties of the module as well as the ambient conditions influence this temperature. These parameters also influence the thermal behavior of the module during the lamination process resulting in a temperature profile through the modules layers. We present a 1-dimensional dynamic model to calculate both the temperature of a solar module in operation as well as during lamination. We analyze the effect of module design (glass-backsheet, glass-glass, full and half cells) as well as bifaciality on the cell temperature during operation. We simulate the lamination process and find the model to be in good agreement with validation measurements. We find significant temperature differences between different module layers.
Keywords: Modelling, Thermal Performance, CTM, Simulation, Photovoltaic Module, Manufacturing, Temperature, Lamination, Operation, Heat Exchange, Half Cell, Bifaciality, Glass-Glass, Albedo

1 INTRODUCTION

The temperature of crystalline solar cells is a relevant factor influencing the power output of photovoltaic modules [1]. Power losses of 0.2% to 0.5% per Kelvin difference to 25 °C (standard testing conditions STC) are typical and nominal module operating temperature (NMOT) of approximately 45 °C can be found in module datasheets. Therefore, power losses due to elevated temperatures can be expected in module operation [2]. Secondly, elevated temperatures accelerate degradation processes [3]. Thirdly, thermal behavior of the photovoltaic module is relevant for module production [4, 5]. Heat transfer within the module during lamination affects actual temperatures in the laminate and therefore the curing process of polymer encapsulants.

Novel cell and module concepts (bifacial cells, glass-glass modules etc.) feature a different behavior regarding electrical, optical and thermal aspects compared to concepts which dominated the markets in the past. The implementation of these new concepts has an influence on the cell temperature, which impacts the power output and yield [6–8].

It is therefore necessary to have a flexible thermal model to evaluate the impact of changes in module design on the operating temperature.

Different models to calculate the module temperature have been presented earlier [9–14]. They mostly do not have the capability to consider different module and component designs (i.e. variation in layer thicknesses). Recently, more advanced models have been proposed that allow the consideration of novel module designs or changes in components [15–17]. We use a similar approach and present a model to calculate temperatures within photovoltaic modules. We combine this model with a set of already established other models (i.e. cell-to-module analysis, optical and electrical modelling of PV modules) [18–22] to allow for a holistic evaluation of module designs [23].

The lamination temperature and process time are key factors in module production. They influence module reliability and costs. It is therefore interesting to optimize this process step. Process targets may not always be fully met due to imperfections in process control and machine design (i.e. positioning of temperature sensors). Hence, deviations between a desired and an actual temperature in a laminate occur. A flexible thermal model is therefore necessary to analyze the heat flows in PV modules and their effects on the encapsulant curing (lamination).

We present such a model and show results regarding the calculation of module temperatures.

In the following we introduce the thermal model and the underlying fundamental equations of heat transfer. Furthermore, we distinguish between the modelling of module operation and lamination. For validation we compare the calculated temperatures with the results of various temperature measurements within the module and on its surface.

2 THERMAL MODEL

We propose a one-dimensional, dynamic model consisting of n layers S_i. Each layer can be a fluid or a solid of a defined material and thickness. A temperature ϑ_j is assigned to each interface F_j bounding the layers. By determining the heat flows inside and on the surfaces of the module a thermal equilibrium can be found at each interface. Solving the set of equations that result from the thermal equilibrium leads to a one-dimensional temperature distribution along the module interfaces.

We differentiate between heat generation q_{source}, dissipation q_{sink}, storage q_s and heat transfers $q_{a \to b}$ that occur between the interfaces as well as between the module and the environment $q_{0 \to 1}$ and $q_{m \to \infty}$.
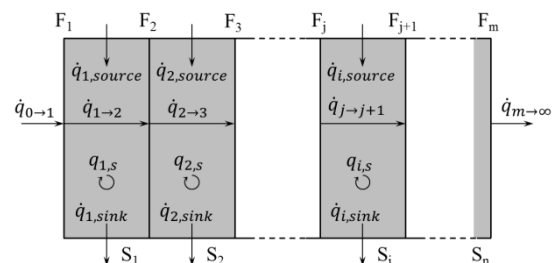
Figure 1: Thermal model with interfaces F, layers S and heat fluxes q

Each layer is characterized by a thickness and its material properties, which are optical parameters (e.g. transparency and emissivity for heat radiation), thermal parameters (i.e. heat conductivity and heat capacity) and mechanical parameters (i.e. mass density). It is possible

to model a physical layer (e.g. a polymer sheet) by using several virtual layers in the model.

The material properties are considered as temperature or spectral dependent values. Thermal parameters and mass density (that depend directly on the material temperature) are interpolated to fit the mean layer temperature. Furthermore, the layer temperature is used to calculate a spectrum of heat radiation according to Planck's Law of black body radiation. Using this spectrum, the optical quantities (that vary with the wavelength) are adjusted to fit the mean layer temperature.

Additional inputs are generated using complementary models [18, 20, 22]. Of especial importance is the absorbed light in each layer (optical model) which acts as a heat source and the electrical power output of the solar cell (electrical model) which is an effective heat sink.
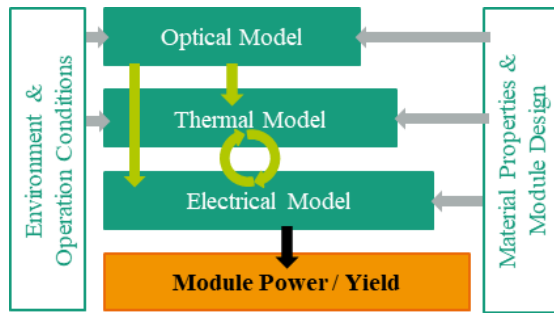
Figure 2: The thermal model and other relevant models to calculate the module power

During calculation, feedback loops may occur since interdependencies exist between power and heat generation (Figure 2) [24].

Therefore, the model follows an iterative structure. Based on an initial temperature distribution along the module layers the temperature dependent quantities are updated. This applies to the material properties as mentioned above as well as to the electrical module power and the Nusselt numbers for convective heat transfer. With the updated values an energy balance is created and solved to calculate the temperature distribution in the module. Using these temperatures the temperature dependent data is updated again leading to a new temperature distribution.

In stationary calculations the model iterates until a desired accuracy in terms of the difference between the current and the previous temperature is reached. A simple, empirical model is used to define an initial guess for the first iteration based on the ambient temperature ϑ_{amb}, the irradiance E and the wind speed v_{wind} [25].

$$\vartheta_{module} = \vartheta_{amb} + \frac{E}{30.02 + 6{,}28 \cdot v_{wind}} \quad (1)$$

However, the model also allows dynamic calculations. In this case the initial temperature distribution equals the start temperatures at the beginning of the simulated time range. Iterations represent a time step of a user-defined length. The model iterates until the desired simulation time is reached.

In order to calculate the module temperatures each interface is considered as a black box with incoming and outgoing heat flows. We differentiate between heat sinks

(q_{sink}), sources (q_{source}), transfers (q_{out}, q_{in}) and storage (q_s).

According to the first law of thermodynamics the sum of these energy flows equals zero for each interface (thermal equilibrium):

$$\sum \dot{q}_j = \dot{q}_{sink} - \dot{q}_{source} + \dot{q}_{out} - \dot{q}_{in} + \frac{q_s}{dt} = 0 \quad (2)$$

Creating this energy balance for each interface leads to a set of m equations based on the unknown layer temperatures.

Electrical energy generation of the photovoltaic cells is considered as a heat sink. Therefore, the module power is calculated in the electrical model that is part of the mentioned feedback loop. Additional heat sinks (e.g. PV module cooling systems) can be added.

Heat transfer comprises of heat conduction, heat radiation exchange and convection.

Heat conduction within (solid) layers can be calculated using the following equation with the interface temperatures ϑ, the layer thickness d and an intermediate heat conductivity λ_m [26]:

$$\lambda_m = \frac{1}{2}\big(\lambda(\vartheta_1) + \lambda(\vartheta_2)\big) \quad (3)$$

$$\dot{q}_{j \to j \pm 1} = \frac{\lambda_m}{d} \cdot \big(\vartheta_j - \vartheta_{j \pm 1}\big) \quad (4)$$

Heat radiation exchange of two parallel surfaces of equal size, the extent of which is significantly greater than their distance can be calculated using [27]:

$$\dot{q}_{j \to j \pm 1} = \frac{\sigma}{\frac{1}{\varepsilon_j} + \frac{1}{\varepsilon_{j \pm 1}} - 1} \cdot \big(T_j^4 - T_{j \pm 1}^4\big) \quad (5)$$

The heat flow depends on the Planck constant σ as well as on the interfaces' emissivities ε and absolute temperatures T.

In addition to heat transfers from interface F_j to the adjacent interfaces F_{j-1} and F_{j+1}, thermal radiation to the more distant interfaces is considered as long as all irradiated layers in between are transparent. As radiation passes through multiple layers of solids, the radiative flux decreases due to absorption. This decline in flux is implemented according to Beer-Lambert law using attenuation coefficients μ [28].

$$\dot{q} = \dot{q}_0 \cdot e^{-\mu * d} \quad (6)$$

Heat storage represents the remaining term in the thermal equilibrium (2). Assuming purely sensible heat the stored energy depends on the mass density ρ, the specific heat capacity c_p and the temporal temperature difference [29]:

$$q_s = \rho \cdot c_p \cdot \big(\vartheta(t + dt) - \vartheta(t)\big) \quad (7)$$

When simulating stationary systems no heat storage is considered as the temporal temperature difference is zero.

Equations (4) to (7) are used to calculate the heat transfers within the photovoltaic module. However, to ensure solvability the one-dimensional layer model requires a boundary condition on each side. This

boundary condition is formed by an interface of a known temperature.

In case of module lamination the first interface represents the laminator cover. Assuming an adiabatic system the interface temperature is fixed to be the known room temperature. The laminator hot plate is representing the last interface accordingly. The hot plate temperature is depending on the lamination process and therefore it is a known input as well.

Modelling the module operation the boundary conditions result from the environmental parameters namely the ambient air and ground temperatures ϑ_{air} and ϑ_g. We consider radiative and convective heat transfer between the module surfaces and the environment.

The heat radiation exchange between a body and its significantly greater environment simplifies to [30]:

$$\dot{q}_{mod \to amb} = \varepsilon_{mod} \cdot \varepsilon_{amb} \cdot \varphi \cdot \sigma \cdot (T_{mod}^4 - T_{amb}^4) \quad (8)$$

Each module surface is represented by its emissivity ε_{mod} and temperature T_{mod} that represent the values for the front side or the backside, respectively. Regarding the ambient parameters ε_{amb} and T_{amb} we differentiate between the values for ground and sky. While ground temperature and emissivity are usually known model inputs we use the following approximations to calculate the equivalent sky parameters [30, 31]:

$$T_{Sky} = 0.0552 \cdot T_{air}^{1;5} \quad (9)$$
$$\varepsilon_{Sky} = 0.72 + 0.005 \cdot \vartheta_{air} \quad (10)$$

Other models are known to describe sky temperature and emissivity and may be used as well [30, 32–34].

For each combination of heat transfer a view factor is defined that takes into account the orientation of the module plane towards the environmental plane. The view factors depend on the module inclination to the horizontal (γ) [30]:

$$\varphi_{front \to sky} = \frac{1}{2} \cdot (1 + \sin(90 - \gamma)) \quad (11)$$

$$\varphi_{front \to ground} = \frac{1}{2} \cdot (1 - \sin(90 - \gamma)) \quad (12)$$

$$\varphi_{back \to sky} = \frac{1}{2} \cdot (1 - \cos \gamma) \quad (13)$$

$$\varphi_{back \to ground} = \frac{1}{2} \cdot (1 + \cos \gamma) \quad (14)$$

In addition to the radiative energy flow heat is transferred from the module surfaces through convection. Heat convection at interfaces with contact to fluids can be calculated using the Nusselt Number Nu, a characteristic length L and the heat conductivity λ [26]:

$$\dot{q}_{j \to fluid} = \frac{Nu_{mix} \cdot \lambda_{fluid}}{L} \cdot (T_j - T_{fluid}) \quad (15)$$

$$L = \begin{cases} h & \text{für } \gamma_E > 0 \\ A/U & \text{für } \gamma_E = 0 \end{cases} \quad (16)$$

The characteristic length L is the height h of the module for non-horizontal operation and the ratio of module area A and circumference U for horizontal mounting [27].

Free and forced convection as well as turbulent and laminar flow can be distinguished and influence the Nusselt number. Free convection is fluid movement after

density and buoyancy changes due to temperature effects. Forced convection describes the influence of wind.

$$Nu_{free} = f(Pr, Ra) \quad (17)$$
$$Nu_{forced} = f(Pr, Re) \quad (18)$$

Prandtl (Pr) and Rayleigh (Ra) numbers vary with the fluid properties and the body geometry.

$$Pr = \frac{c_p \cdot \eta}{\lambda} = \frac{\upsilon}{a} \quad (19)$$
$$Ra = Gr \cdot Pr \quad (20)$$
$$Gr = \frac{g' \cdot \beta \cdot L^3 \cdot (T_2 - T_1)}{\nu} \quad (21)$$

c_P – specific heat capacity, η - dynamic viscosity, λ - heat conductivity, υ - kinematic viscosity, a - thermal diffusity, g' – vertical component of the gravitational acceleration, β - coefficient of isobaric volume expansion, L - characteristic length

Convection within a photovoltaic module is theoretically possible in gas-filled modules [35, 36]. However, due to the typically low thickness of fluid module layers in such designs, conductive transfer according to (4) is assumed for the heat flow. To assess, if a layer is a thin and conductive heat transfer can be assumed, we use the criteria Ra < 1707 [30, 37, 38].

Convection does not take place in solid materials. Therefore, this consideration is only relevant for special gas-filled modules and is not used below.

Forced convection on the outside of modules is calculated using the Reynolds number Re which is a function of the flow speed (e.g. the wind speed).

Free and forced convection occur at the same time in operation and a mixed Nusselt number has to be used considering both. On the module front the '+' has to be used and on the module rear the '-' [27].

$$Nu_{mix} = \sqrt[3]{Nu_{forced}^3 \pm Nu_{free}^3} \quad (22)$$
with $0.1 < Pr < 100$

The compensation of free and natural convection on the module rear side is valid as long as $Nu_{free} < 0.8 \cdot Nu_{forced}$. If the Nusselt number of free convection is larger, Nu_{free} has to be used instead of Nu_{mix}.

The Nusselt number of free convection from a plane to the air underneath the plane (e.g. the heat transfer from the module back side) is calculated using the inclination γ [27]:

$$Nu_{free,laminar} = \left(0.825 + 0.387 \cdot \sqrt[6]{K}\right)^2$$
$$K = Ra \cdot \cos \gamma \cdot \left[1 + \left(\frac{0.492}{Pr}\right)^{9/16}\right]^{-16/9} \quad (23)$$
with $0.1 < Ra < 10^{12}$ and $Pr > 0.001$

For the module front side (23) can only be used for laminar flow. The critical Rayleigh number Ra_{crit} describes the transition from laminar to turbulent flow. For $Ra > Ra_c = 10^{8,9 - 0,00178 * \gamma^{1,82}}$ the Nusselt number for turbulent flow is used [27]:

$$Nu_{free,turbulent} = 0.56 \cdot \sqrt[4]{Ra_c * \cos\gamma} + 0.13 \\ \cdot \left(\sqrt[3]{Ra} - \sqrt[3]{Ra_c}\right) \tag{24}$$

In addition to the heat transferred through free convection forced convection occurs due to wind. The respective Nusselt numbers are calculated using (25) to (27) [27].

$$Nu_{forced} = \sqrt{Nu_{forced,lam.}^2 + Nu_{forced,turb.}^2} \tag{25}$$

with $10 < Re < 10^7$ and $0.6 < Pr < 2000$
$$Nu_{forced,lam.} = 0.664 \cdot \sqrt{Re} \cdot \sqrt[3]{Pr} \tag{26}$$

with $Re < 10^6$
$$Nu_{forced,turb.} = \frac{0,037 \cdot Re^{0,8} \cdot Pr}{1 + 2.443 * Re^{-0,1} \cdot (Pr^{2/3} - 1)} \tag{27}$$

with $10 < Re < 10^7$ and $0.6 < Pr < 2000$

During heat transfer between two bodies, described by the correlations described above, temperature changes temporally and spatially resolved. If a body absorbs heat without changing chemically or undergoing a phase transition, we can describe the relation between temperature change and heat storage using [29]:

$$Q = m * c_p * \left(\vartheta(t + dt) - \vartheta(t)\right) \tag{28}$$

We calculate a specific heat density by dividing with the area (ρ_m – density of the body):

$$q = \rho_m * d * c_p * \left(\vartheta(t + dt) - \vartheta(t)\right) \tag{29}$$

Important inputs for the modelling of the module operation temperature are heat sources from the absorption of light and electrical heating from resistive losses. At the same time the electrical power output of the module acts as a heat sink. We combine the thermal model with the models used in SmartCalc.CTM to calculate heat sources and sinks [18, 19, 21, 22, 39].

Heat sinks and sources are attributable to module layers but the thermal model is based on heat exchange between interfaces. We therefore distribute heat sinks and sources equally from layers to their adjacent interfaces.

3 MODULE OPERATION

We calculate the cell temperature of modules of different design and evaluate the differences in temperature with respect to the module output power. We compare a module with full and with halved solar cells as well as modules with a white polymer backsheet and a transparent glass rear cover. We perform additional calculations considering bifaciality and rear side irradiance (albedo). Bifaciality of the solar cell is set to 90% of the front side I_{MPP} without assuming additional effects on the solar cell. If applicable, an albedo of $A = 0.2$ is used for calculations. The rear side irradiance is assumed to be totally diffuse while front side irradiance is direct and perpendicular.

Material parameters and module design are based on commercially available products. We choose the glass-glass setup to have two 2 mm thick glasses, while the

glass-foil-design has a 3 mm front glass. Ambient temperature is set to 25 °C, wind speed to 1 m/s and module inclination to 45°. All submodels have been integrated into a global model (SmartCalc.CTM version 1.2.1) as shown in Figure 2.

Temperature calculation results are shown in Table 1.

Table 1: Cell temperatures [°C] of different modules at different irradiances. HC = half cell, FC = full cell, BS = glass-backsheet module setup, GG = glass-glass module setup, mono = monofacial, bifa = bifacial, A = albedo.

irradiance [W/m²]	200	400	600	800	1000	1200
FC, BS, mono, A=0	29.8	37.2	44.5	51.7	58.9	66.1
HC, BS, mono, A=0	29.8	37.3	44.6	51.8	58.9	66.1
FC, GG, mono, A=0	29.3	36.2	42.9	49.7	56.4	63.0
HC, GG, mono, A=0	29.3	36.1	42.9	49.5	56.1	62.7
FC, BS, bifa, A=0	29.8	37.2	44.5	51.7	58.9	66.1
HC, BS, bifa, A=0	29.8	37.2	44.5	51.8	58.9	66.0
FC, GG, bifa, A=0	29.3	36.2	42.9	49.7	56.4	63.0
HC, GG, bifa, A=0	29.3	36.1	42.9	49.5	56.1	62.7
FC, BS, mono, A=0.2	30.2	38.0	45.6	53.2	60.8	68.3
HC, BS, mono, A=0.2	30.2	38.0	45.7	53.3	60.8	68.3
FC, GG, mono, A=0.2	30.8	39.1	47.3	55.4	63.4	71.4
HC, GG, mono, A=0.2	30.8	39.1	47.3	55.3	63.2	71.1
FC, BS, bifa, A=0.2	30.2	38.0	45.6	53.2	60.8	68.3
HC, BS, bifa, A=0.2	30.2	38.0	45.7	53.3	60.8	68.2
FC, GG, bifa, A=0.2	30.5	38.6	46.5	54.4	62.2	70.0
HC, GG, bifa, A=0.2	30.5	38.5	46.4	54.2	61.9	69.6

As expected, we find the cell temperatures do be dependent on irradiance and module setup. We use the full cell (FC), glass-backsheet (BS) monofacial (mono) module with no albedo (A=0) as a reference. We compare half-cell (HC), glass-glass (GG) and bifacial (bifa) modules with that reference and calculate the glass-glass module to be significantly cooler than the reference when no albedo is assumed (Figure 3).
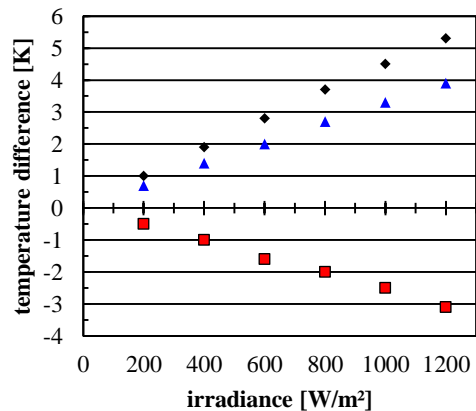
Figure 3: Difference in cell temperature of different glass-glass modules to the reference module (FC, BS, mono, A=0)

The effective thermal resistance of glass is higher than the backsheet even though it has a higher thermal conductivity. Its thickness compensates the advantage and module glass is a more effective thermal barrier. Therefore, we would expect that the glass-glass module has a higher temperature. However, we observe the opposite as shown in Figure 3.

We find this effect to be related to the energy absorbed in the module. Firstly, glass allows light to pass through the module in the cell spacing areas of the module without being absorbed and without acting as a heat source. Secondly, since there is a reduction in internal reflection, also the other layers have a lower absorption. The heating after internal reflection is especially relevant when looking at the solar cell which is a strong absorber of light. White backsheets that reflects light onto the solar cell and has a significant impact on module power [39]. Assuming a cell efficiency of 20% and a low reflectivity of the solar cell, we can roughly estimate that for every Wp in backsheet gains, almost 4 Wp have to be considered as a heat source. We conclude that an increase in module efficiency based on optical cell-to-module gains may lead to an increase in module power and an increase in temperature at the same time due to thermalization in the solar cell.

We see the effect of the higher effective thermal resistance of glass when analyzing layer temperatures in detail (Figure 4). The higher thermal resistance of the glass leads to a higher temperature drop in the rear glass (0.6 K) than in the backsheet (0.3 K). Nonetheless, we calculate the glass-glass module to be significantly cooler than the glass-foil module when no albedo is present due to the effects described above.
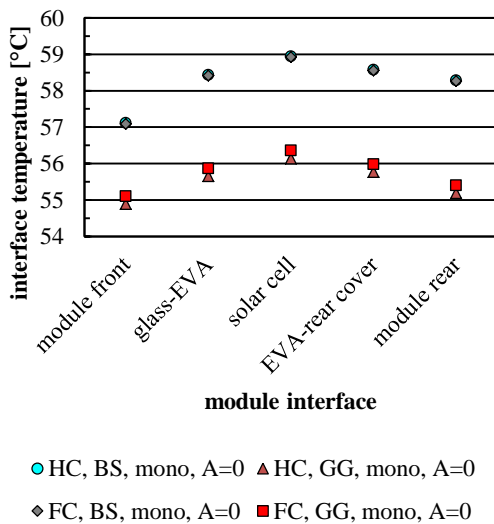
Figure 4: Layer temperatures in different module setups.

With additional rear side irradiance (A=0.2), the glass-glass module becomes warmer than the reference due to an increase in absorbed light. With a transparent rear glass, additional light is entering the module which causes heating. The white backsheet has a higher reflectivity thus reducing the temperature compared to the glass-glass module for albedo conditions. Compared to the reference, the additional heating from the absorption of albedo in the backsheet leads to higher temperatures (Table 1).
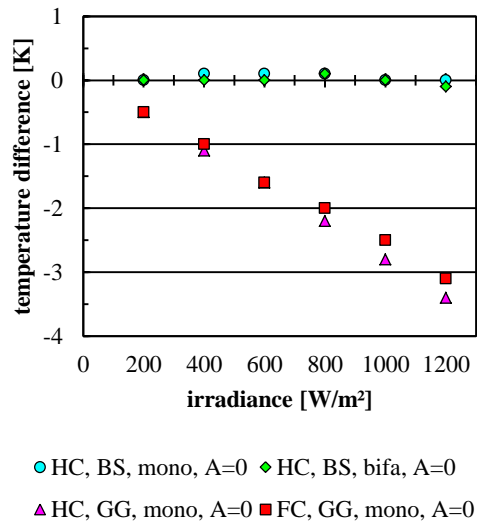
Figure 5: Difference in cell temperature of different glass-glass modules to the reference module (FC, BS, mono, A=0).

We compare full cell and half cell designs and find half cell modules to be at a similar temperature as their respective full cell module equivalent (Figure 5).

Different effects occur that influence the temperature:

Firstly, the half cell module converts more light into electrical power thus increasing a heat sink. Secondly, effects from heating through electrical losses are reduced for half cells. Lower currents lead to lower electrical losses [40] which are a heat source. Thirdly, as discussed above, internal reflection within the module, subsequent absorption and imperfect power generation in the solar cell causes heating. Half cells usually feature more cell spacing area and thus additional heating after internal reflection is more relevant.

Due to the rear glass, internal reflection gains are small for both cell concepts and heat sources from internal reflection are reduced. The advantage of half cells regarding module power is lower due to missing reflection power gains but half cells still have a higher power output since the electrical losses are lower. We consequently find the glass-glass half cell module to be cooler than the full cell equivalent.

When considering bifaciality, all effects described above occur as well: currents are increased due to higher irradiance leading to higher electrical losses. At the same time also more electrical power is generated (limited by the cell efficiency) which acts as a heat sink.

Our calculations show similar temperatures of mono- and bifacial cells if no albedo is present (Figure 5). We find a small increase in module power for modules with bifacial cells even if an opaque backsheet is used due to additional internal reflection gains (Figure 6) [20, 39]. This increase in power (< 0.2%) acts as a heat sink. At the same time, thermalization losses after internal reflection will increase for bifacial cells. Both effects are small and therefore module temperatures are similar.

If albedo is considered, bifaciality of solar cells reduces the module temperature for transparent rear covers due to additional power generation compared the monofacial cells (Table 1).
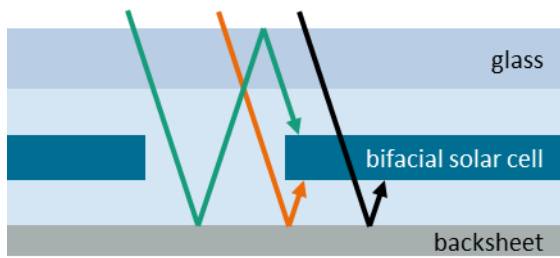
Figure 6: Cover coupling gains in monofacial modules with bifacial cells

We assume a front irradiance of 1000 W/m² and no albedo. We calculate the total energy absorbed by the reference module to be 892 W/m² while the rest is reflected at front glass, solar cell and inactive module area. Heat generation resulting from the imperfect energy conversion of the absorbed light in the solar cell is the main heat source during module operation.

We perform a variation of the wind speed between 0 and 5 m/s, which impacts the module temperature but not the energy absorption. The electrical power output changes with cell temperature in each scenario and is calculated to be between 164 and 182 W/m². Therefore between 710 and 728 W/m² have to be dissipated via convection or radiation. We analyze the energy transfer at the outer module interfaces and find the front to be responsible for 52 to 57% of the energy dissipation (without electrical power and reflection). Comparing radiative and convective heat transfer we unsurprisingly find convection to be dominant for higher wind speeds (Figure 7).
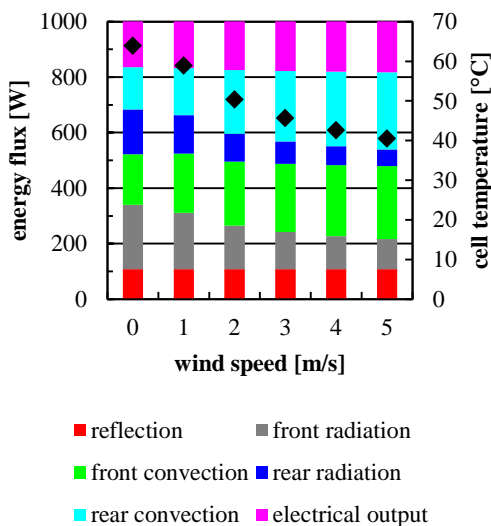
Figure 7: Energy flux from radiation and convection at the module front and rear side for different wind speeds, 1000 W/m², 45° module inclination, 25 °C ambient temperature

4 MODULE LAMINATION

We apply the thermal model to simulate the lamination process of a photovoltaic module in a membrane laminator. The lamination setup is shown in Figure 8.
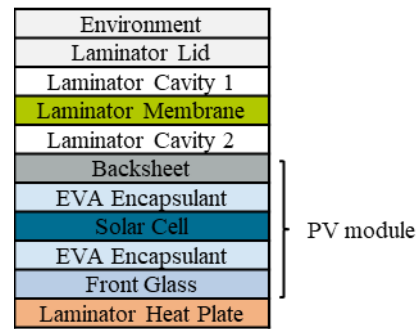
Figure 8: Stack setup for the simulation of the lamination process

The cavities are not permanent. During the lamination process a "pressing" phase is applied where cavity 1 is created between the laminator lid and the membrane. During the same time laminator cavity 2 is closed and a direct contact between membrane and front glass is established.

A lamination experiment is performed using thermocouple temperature sensors in different module layers to validate the model (Figure 9). We use a highly flexible laboratory laminator that has active cooling capabilities. We use the temperature profile as an input and apply the dynamic model considering heat storage for this application. We find differences between the actual equipment temperature profile and the measured data. Modelling the equipment itself is not part of this study. We therefore use the measured laminator temperature as an input for module layer temperature simulation.
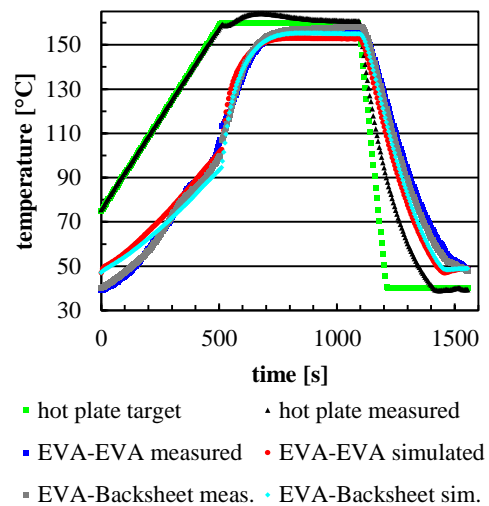
Figure 9: Measured and simulated temperatures in a module stack / at different module interfaces during lamination

Results of simulation and measurement are in good agreement. We calculate a mean error of 2 K for the relevant polymer layers. We find the model to be able to calculate the actual temperatures within the laminate during manufacturing using material parameters, a module stack and lamination process parameters.

■ hot plate (measured) • glass-EVA
• EVA-EVA ▲ EVA-backsheet
• backsheet outside
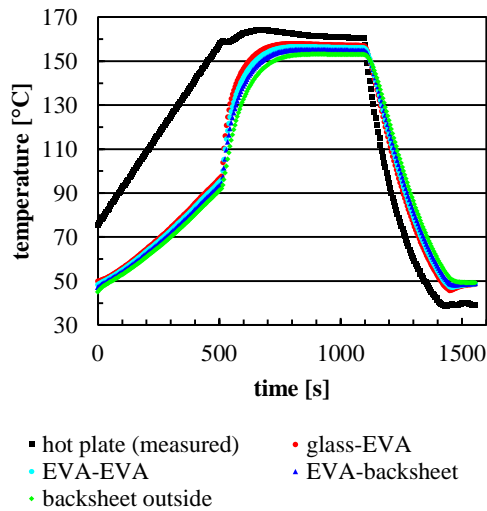
Figure 10: Simulated temperatures at different module interfaces

We analyze the temperature in different module layers and find them to be different from each other (Figure 10). At 900 seconds process time ("cure" / "hold" process step) a difference of 2.5 K can be observed between the glass-encapsulant and the backsheet-encapsulant interface. The mean difference between both layers is 1.3 K. It is known that the curing reaction is strongly dependent on the encapsulant temperature. Therefore differences between module layers may lead to different degrees in crosslinking. Even more critical is the difference between the desired process temperature (as programmed in the laminator control) and the actual temperature reached within the module stack.

We therefore conclude from our simulation results that a detailed analysis of the lamination process is necessary for every module setup to find an optimal process for the complete module stack.

5 SUMMARY

We present a thermal model to calculate layer temperatures in PV modules. The model is one dimensional and considers environmental parameters as well as material and geometrical data of the individual layers in a PV module. Both static and dynamic calculations are possible due to implementation of heat storage terms.

We integrate the thermal model into a simulation environment containing optical and electrical models ("SmartCalc.CTM"). Doing so, we are able to calculate the module layer temperatures at realistic operation conditions (ambient temperature, wind speed etc.) for different module setups considering cell-to-module power gains and losses. The optical and geometrical models are used to calculate heat sources (i.e. absorption in layers) as well as heat sinks (i.e. electrical power generation).

We compare different module designs (full cell / half cell, glass-glass / glass-backsheet, monofacial / bifacial) regarding their temperature at different operation conditions. We perform a variation of irradiance (200-1200 W/m; with / without additional albedo) and calculate the cell temperature for each setup.

We calculate glass-glass modules to be cooler than the glass-backsheet design when no albedo is considered since the transparent rear glass reduces absorption of light within the module. If albedo is considered, light entering through transparent rear covers and subsequent absorption in the module will result in higher module temperatures.

We identify backsheet gains and related absorption in the solar cell to be a highly relevant factor in the heating of modules.

For bifacial module designs (i.e. glass-glass), bifaciality of solar cells reduces the operating temperature compared to monofacial cells. The use of bifacial solar cells in modules with opaque rear covers does not significantly impact module temperature.

We find half cell modules to be not generally cooler than comparable full cell module designs. While the temperature of half cells is lower than for full cells in glass-glass modules, for white backsheets no such general advantage has been calculated.

We apply the thermal model to a lamination process to calculate the respective layer temperatures during lamination (mean error = 2 K). We calculate a mean temperature difference between the EVA and the backsheet to be 1.3 K to during the process. Since the crosslinking processes in the encapsulants are temperature sensitive, a detailed analysis of layer temperatures is advised.

REFERENCES

[1] O. Dupré, R. Vaillon, and M. A. Green, "Physics of the temperature coefficients of solar cells," *Sol Energ Mat Sol C*, vol. 140, pp. 92–100, 2015.

[2] T. Nordmann and L. Clavadetscher, "Understanding temperature effects on PV system performance," in *Proceedings of the 3rd IEEE World Conference and Exhibition on Photovoltaic Energy Conversion*, Osaka, Japan, 2003, pp. 2243–2246.

[3] C. Ferrara and D. Philipp, "Why do PV modules fail?," in *Proceedings of the International Conference on Materials for Advanced Technologies*, 2011, pp. 379–387.

[4] U. Eitner, S. Kajari-Schroeder, M. Koentges, and H. Altenbach, "Thermal stress and strain of solar cells in photovoltaic modules," in *Advanced Structured Materials*, vol. 15, *Shell-like Structures: Non-classical Theories and Applications*, H. Altenbach and V. A. Eremeyev, Eds., Berlin/Heidelberg: Springer, 2011.

[5] A. J. Beinert *et al.,* "Thermomechanical stress analysis of PV module production processes by Raman spectroscopy and FEM simulation," *Energy Procedia*, vol. 124, pp. 464–469, 2017.

[6] J. Rabanal-Arabach and A. Schneider, "Anti-reflective Coated Glass and its Impact on Bifacial Modules' Temperature in Desert Locations," *Energy Procedia*, vol. 92, pp. 590–599, 2016.

[7] S. Regondi, H. Hanifi, and J. Schneider, "Modeling and Simulation of the Influence of Interconnection Losses on Module Temperature in Moderate and Desert Regions," *IEEE J. Photovoltaics*, pp. 1–7, 2019.

[8] M. R. Vogt *et al.,* "Reduced Module Operating Temperature and Increased Yield of Modules With PERC Instead of Al-BSF Solar Cells," *IEEE J. Photovoltaics*, vol. 7, no. 1, pp. 44–50, 2017.

[9] D. A. Skoog and J. J. Leary, *Instrumentelle Analytik: Grundlagen, Geräte, Anwendungen*: Springer Verlag, 1996.

[10] E. Skoplaki and J. A. Palyvos, "Operating temperature of photovoltaic modules: a survey of pertinent correlations," (English), *Renew Energ*, vol. 34, no. 1, pp. 23–29, 2009.

[11] M. Koehl, M. Heck, S. Wiesmeier, and J. Wirth, "Modeling of the nominal operating cell temperature based on outdoor weathering," (English), *Sol Energ Mat Sol C*, vol. 95, no. 7, pp. 1638–1646, 2011.

[12] M. Mattei, G. Notton, C. Cristofari, M. Muselli, and P. Poggi, "Calculation of the polycrystalline PV module temperature using a simple method of energy balance," *Renewable Energy*, vol. 31, no. 4, pp. 553–567, 2006.

[13] D. Faiman, "Assessing the outdoor operating temperature of photovoltaic modules," *Prog Photovoltaics*, vol. 16, no. 4, pp. 307–315, 2008.

[14] N. A. Zainal, Ajisman, and A. R. Yusoff, "Modelling of Photovoltaic Module Using Matlab Simulink," *IOP Conf. Ser.: Mater. Sci. Eng.*, vol. 114, p. 12137, 2016.

[15] A. Thomson, M. Ernst, I. Haedrich, and J. Qian, "Impact of PV module configuration on energy yield under realistic conditions," *Opt Quant Electron*, vol. 49, no. 2, p. 329, 2017.

[16] H. Hanifi, C. Pfau, M. Turek, and J. Schneider, "A practical optical and electrical model to estimate the power losses and quantification of different heat sources in silicon based PV modules," *Renewable Energy*, vol. 127, pp. 602–612, 2018.

[17] M. R. Vogt, H. Holst, M. Winter, R. Brendel, and P. P. Altermatt, "Numerical Modeling of c-Si PV Modules by Coupling the Semiconductor with the Thermal Conduction, Convection and Radiation Equations," *Enrgy Proced*, vol. 77, pp. 215–224, 2015.

[18] M. Mittag *et al.,* "Electrical and thermal modeling of junction boxes," in *Proceedings of the 33rd European Photovoltaic Solar Energy Conference and Exhibition (EU PVSEC)*, Amsterdam, 2017, pp. 1501–1506.

[19] M. Mittag and M. Ebert, "Systematic PV module optimization with the cell-to-module (CTM) analysis software," *Photovoltaics International*, no. 36, pp. 97–104, 2017.

[20] A. Pfreundt, M. Mittag, M. Heinrich, and U. Eitner, "Rapid Calculation of the Backsheet Coupling Gain Using Ray Groups," *32nd European Photovoltaic Solar Energy Conference and Exhibition (EUPVSEC)*, 2018.

[21] M. Mittag *et al.,* "Cell-to-Module (CTM) analysis for photovoltaic modules with shingled solar cells," in *44th IEEE PV Specialist Conference PVSC*.

[22] I. Hädrich, U. Eitner, M. Wiese, and H. Wirth, "Unified methodology for determining CTM ratios: Systematic prediction of module power," *Sol Energ Mat Sol C*, vol. 131, pp. 14–23, 2014.

[23] M. Mittag *et al.,* "Approach for a Holistic Optimization from Wafer to PV System," in *Proceedings of the 7th World Conference on Photovoltaic Energy Conversion*, Hawaii, 2018.

[24] H. Hanifi and J. Schneider, "Evaluation of Different Module Designs and Determination of Different Physical Loss Mechanisms by Practical Means of a Practical Multi-Physic Model," in *35th European Photovoltaic Solar Energy Conference and Exhibition*.

[25] C. Schwingshackl *et al.,* "Wind Effect on PV Module Temperature: Analysis of Different Techniques for an Accurate Estimation," *Energy Procedia*, vol. 40, pp. 77–86, 2013.

[26] P. v. Böckh and T. Wetzel, *Wärmeübertragung: Grundlagen und Praxis,* 5th ed. Berlin: Springer, 2014.

[27] VDI - Verein Deutscher Ingenieure, *VDI-Wärmeatlas*. Berlin, Heidelberg: Imprint: Springer Vieweg, 2013.

[28] J. Eichler, *Physik: Grundlagen für das Ingenieurstudium - kurz und prägnant ; mit 54 Tabellen ; [jetzt mit über 250 Übungsaufgaben + Lösungen],* 3rd ed. Wiesbaden: Vieweg, 2007.

[29] M. Sterner and I. Stadler, *Energiespeicher - Bedarf, Technologien, Integration*. Berlin: Springer Vieweg, 2014.

[30] S. Krauter, *Solar Electric Power Generation: Modeling of Optical and Thermal Performance, Electrical Yield, Energy Balance, Effect on Reduction of Greenhouse Gas Emissions*: Springer-Verlag, 2006.

[31] P. J. Craul, *Urban Soils: Applications and Practices*: John Wiley & Sons, 1999.

[32] S. A. Al-Sanea, M. F. Zedan, S. A. Al-Ajlan, and A. S. Abdul Hadi, "Heat Transfer Characteristics and Optimum Insulation Thickness for Cavity Walls," *Journal of Thermal Envelope and Building Science*, vol. 26, no. 3, pp. 285–307, 2003.

[33] O. Gliah, B. Kruczek, S. G. Etemad, and J. Thibault, "The effective sky temperature: an enigmatic concept," *Heat Mass Transfer*, vol. 47, no. 9, pp. 1171–1180, 2011.

[34] J. Sedlar and R. Hock, "Testing longwave radiation parameterizations under clear and overcast skies at Storglaciären, Sweden," *The Cryosphere*, vol. 3, no. 1, pp. 75–84, 2009.

[35] M. Mittag, U. Eitner, and T. Neff, "TPedge: progress on cost-efficient and durable edge-sealed PV modules," in *Proceedings of the 33rd European Photovoltaic Solar Energy Conference and Exhibition (EU PVSEC)*, Amsterdam, 2017, pp. 48–54.

[36] D. Reinwand *et al.,* "All Copper NICE Modules," in *Proceedings of the 7th World Conference on Photovoltaic Energy Conversion*, Waikoloa Village, HI, USA, 2018, pp. 628–631.

[37] Verein Deutscher Ingenieure (VDI) and VDI-Gesellschaft Verfahrenstechnik und Chemieingenieurwesen (GVC), *VDI-Wärmeatlas,* 10th ed. Berlin/Heidelberg: Springer, 2006.

[38] J. A. Duffie and W. A. Beckman, *Solar engineering of thermal processes,* 2nd ed. New York: Wiley, 1991.

[39] M. Mittag *et al.,* "Analysis of backsheet and rear cover reflection gains for bifacial solar cells," *33rd European PV Solar Energy Conference and Exhibition*, vol. 2017.

[40] M. Mittag, A. Pfreundt, J. Shahid, N. Wöhrle, and D. H. Neuhaus, "Techno-Economic Analysis of Half Cell Modules: The Impact of Half Cells on Module Power and Costs," in *36th European Photovoltaic Solar Energy Conference and Exhibition (EU PVSEC)*.